JOURNAL OF MATERIALS SCIENCE 15 (1980) 1889–1897

Mechanical behaviour of polycrystalline BeO, Al_2O_3 and AlN at high pressure

H. C. HEARD, C. F. CLINE
University of California, Lawrence Livermore Laboratory, Livermore, California 94550, USA

The mechanical behaviour of various types of BeO, Al_2O_3, and AlN have been investigated at confining pressures up to 1.25 GPa, at 25° C, and at strain rates of 3 to 7 x 10^{-5} sec^{-1}. The stress–strain data taken in uniaxial compressive-stress loading indicate the BeO aggregates undergo a transition from brittle fracture at low pressures to plastic flow at high pressures. Depending on the fabrication process, this transition pressure in BeO occurs at 0.4 to 0.7 GPa. Concurrently, the ultimate compressive strength of BeO increases from 1.0 to 1.9 GPa at 0.1 MPa pressure to over 4.0 GPa at 1.0 GPa. Alumina remains brittle at all pressures up to 1.25 GPa; its strength increases from 4.5 GPa at 0.1 MPa pressure to over 6.0 GPa at 1.25 GPa. Aluminium nitride behaves similarly to BeO, having a brittle–ductile transition at 0.55 GPa. Its ultimate strength increases from 3.2 GPa at 0.1 MPa pressure to 4.7 GPa at 0.8 GPa. The distortional strain energy (proportional to the area under the stress–strain curve) absorbed by each material during compression at pressure was calculated and compared to available data from the literature. Alumina shows a degraded energy absorption with pressure, but both BeO and AlN yield a strongly enhanced performance at moderate pressures. Beryllium oxide and AlN thus appear to be promising structural materials for certain applications where high strengths and ductilities are required at moderate pressures.

1. Introduction

The motivation for studying high-pressure mechanical properties of BeO, AlN, and Al_2O_3 originated during our work on the physics of ballistic penetration of light armour by steel projectiles [1]. These ballistic-impact data indicated superior performance of BeO and AlN over Al_2O_3 (especially on a density x thickness basis). The data could not be rationalized by a purely elastic response. Because most naturally occurring oxides and silicates exhibit a transition from elastic behaviour at ambient pressures to a plastic response at high pressures, it was hypothesized that the superiority of BeO and AlN over Al_2O_3 could result from a similar increase in ductility and strength at the high pressures ahead of the projectile. We felt that a tractable approach to understanding the impact conditions involving a large deviatoric stress, a high pressure, and a high strain rate ($\sim 10^3$ sec^{-1}) was to explore these variables through carefully controlled laboratory compression studies. Owing to their excellent thermal, mechanical, and corrosion properties, BeO, AlN, and Al_2O_3 are also of interest as high-strength or high-temperature structural materials. Thus, engineers involved in structural applications (such as in turbine blades and rotors, draw dies, or cutters) might be interested in such materials because of their relatively high impact resistance.

Evidence for change in physical (especially mechanical) properties with modified conditions of deformation environment may be found largely in the physics, engineering, and earth sciences literature. Such studies demonstrate that in a single crystal or in a single-phase or multiphase polycrystalline aggregate, both compressive strengths and ductility may be enormously enhanced be deformation under a superposed

0022–2461/80/081889–09$02.90/0

TABLE I Physical characteristics of materials studied

Compound	Fabrication	ρ_0 (g cm^{-3})	Average grain size (μm)	Porosity (%)	Purity (%)
BeO	Hot pressed, 1700° C, 35 MPa	3.00	10	<1	99+
BeO	Cold pressed and sintered	2.85	30	<5	98+
BeO + 4 mol% Al_2O_3	Cold pressed and sintered, 1850° C in H_2	2.95	–	<2	99+
AlN	Hot pressed	3.27	4	<1	95+
Al_2O_3	Hot pressed	3.92	–	<2	99+

hydrostatic pressure [2–4]. In such materials, strength increases with strain rate, but ductility decreases [5–7]. The mechanical response of a single crystal (and hence of the aggregate) is also dependent on crystal structure. Structure can determine the elements most susceptible to deformation, such as cleavage, slip and twin planes together with their direction and sense of displacement. Changes in the physical environment in combination with crystal structure may act to suppress (or favour) change of certain slip systems, thus altering the mechanical response of the material.

Both BeO and AlN are isostructural, having the wurtzite structure with the space group $P6_3MC$. This structure can be thought of as two identical and interpenetrating hexagonal lattices. The two arrays are shifted with respect to each other so that the points of each lattice lie in the centre of the tetrahedral interstices of the other lattice. The cations occupy the points of one lattice and the anions, the points of the other. All the atoms then have tetrahedral co-ordination, with the tetrahedra of one type all pointing in the same direction along the c-axis. The ideal c_0/a_0 ratio [8, 9] for a hexagonal close-packed lattice is 1.633 (i.e. $2\sqrt{2}/\sqrt{3}$); however, most of the wurtzite-type compounds show some deviation from this ideal value. It has been shown that BeO [8, 9] with $c_0/a_0 = 1.622$ and AlN with $c_0/a_0 = 1.600$ have a smaller c/a. This results in a longer bond length in the c direction, which could modify the mechanical properties. Microhardness studies by Cline and Kahn [10] show an orientational dependence on the $(1\,0\,\bar{1}\,0)$ plane. They report a lower hardness when the long axis of the Knoop indenter is aligned parallel to the c-axis compared to a similar measurement perpendicular to the c-axis. This hardness anisotropy is related to the pronounced prismatic cleavage of BeO and AlN and was expected to influence the mechanical behaviour of the aggregates in our high-pressure work.

Alpha Al_2O_3, on the other hand, is rhombohedral with space group $D_3d^6(R\bar{3}c)$. The structure is best pictured as a slightly distorted, hexagonal, close packing of oxygen ions with the smaller aluminium ions in the interstices. Alpha Al_2O_3 does not exhibit a pronounced cleavage and is distinctly harder than BeO or AlN, having a basal plane microhardness of 2000 kg mm^{-2} versus a basal plane hardness of 1300 for BeO and AlN.

2. Materials and methods

Five materials were tested in uniaxial compression at 25° C and up to pressures of 1.25 GPa.* The materials used were hot-pressed BeO, cold-pressed BeO, hot-pressed BeO + 4 mol% Al_2O_3, hot-pressed Al_2O_3, and hot-pressed AlN. Physical characteristics of all five materials are summarized in Table I. All test samples were prepared by diamond coring from the parent material and were jacketed in 0.2 mm copper or lead jackets and compressed to failure at a strain rate of 10^{-4} sec^{-1}. Right-circular cylinders, having a length–diameter ratio of 2 to 2.5, were prepared from these cores. Diameters varied from 0.6 to 0.9 cm.

True stress differences $(\sigma_1 - \sigma_3)$† were computed from the total force applied to the jacketed sample, after correcting for the strength of the jacket at any strain and correcting this true stress for the increased area resulting from straining. Axial strains were computed from initial sample length and piston displacement. Two different deformation apparatuses were employed; each was fitted with an internal-force gauge. Primarily because of load restrictions, the first unit was used on the smaller diameter, weaker materials. This first apparatus [6] has the capability of

*1 GPa = 1000 MPa = 10 kbar = 145 000 psi.

†If σ_1 is taken as the maximum principal stress (axial) and σ_2, σ_3 are the minimum principal stresses (radial and equal to the confining pressure), $\sigma_1 - \sigma_3$ is the stress difference. Compression is taken as positive.

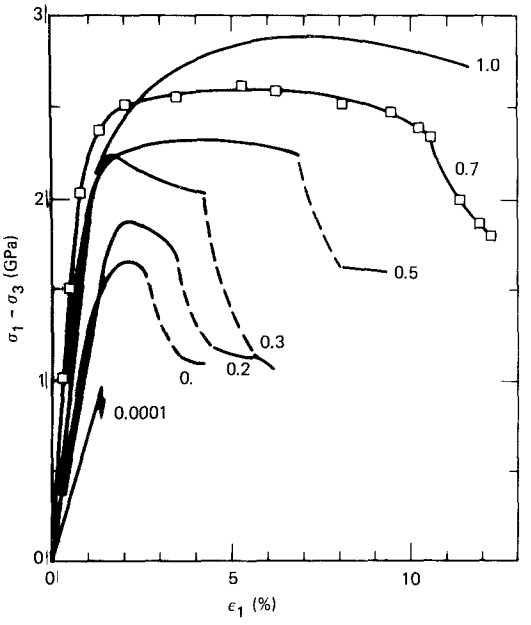

Figure 1 Stress–strain curves for hot-pressed BeO with compression perpendicular (⊥) to parent disc (strain rate from 3 to 7×10^{-5} sec^{-1}). Numbers on curves denote pressure in GPa. Data points shown on 0.7 GPa curves are typical of scatter in stress–strain measurements.

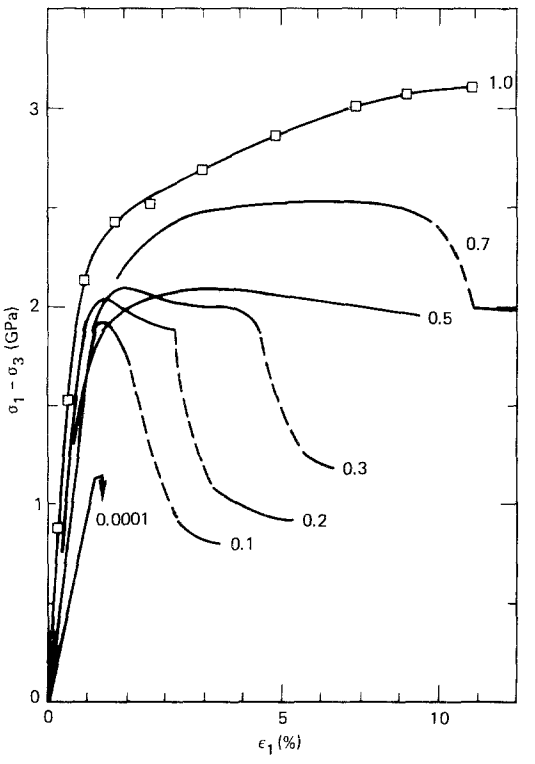

Figure 2 Same as in Fig. 1 but compression 45° to parent disc.

1.0 GPa σ_3 at temperatures to 1000° C and at strain rates ranging from 10^{-2} to 10^{-8} sec^{-1}. The second apparatus [11], employed for all other tests, may be operated to pressures in excess of 2.0 GPa but at strain rates of only 10^{-4} to 10^{-5} sec^{-1}. Accuracy of stress determination (σ_1) in either apparatus is about 20 MPa. The confining pressure in both cases is accurate to about 1.0 MPa or 0.5%, whichever is greater. Accuracy of strains (axial) at the sample is known to 0.2%.

3. Experimental results

Figs. 1 to 3 illustrate the stress–strain behaviour for three orientations of test samples prepared from the first material, hot-pressed BeO, which had a grain size of 10 μm and a porosity of 1%. Hot-pressed BeO has a highly oriented microstructure because of small lath-like crystals, which orient during pressing and control the resulting microstructure. These laths are single crystals elongated parallel to the c-axis. Most laths are preferentially oriented parallel to the plane of the parent disc; thus, most c-axes are radially oriented in the plane of the disc.

Three orientations of samples were tested: σ_1 oriented parallel, σ_1 at 45°, and σ_1 perpendicu-

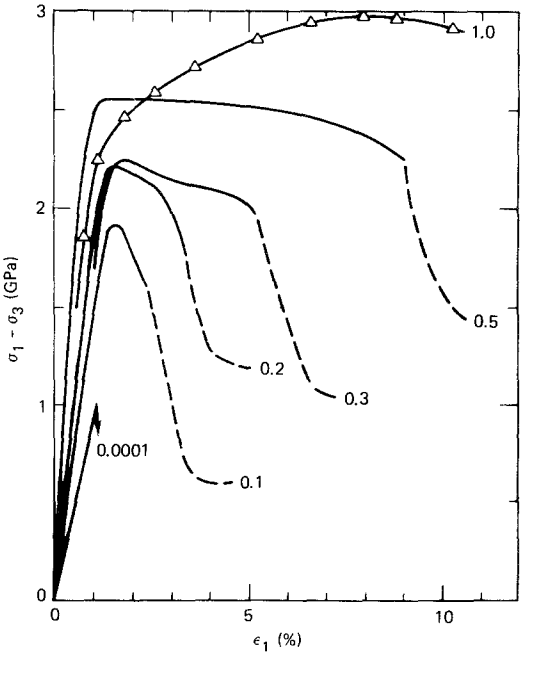

Figure 3 Same as in Fig. 1 but compression parallel (∥) to parent disc.

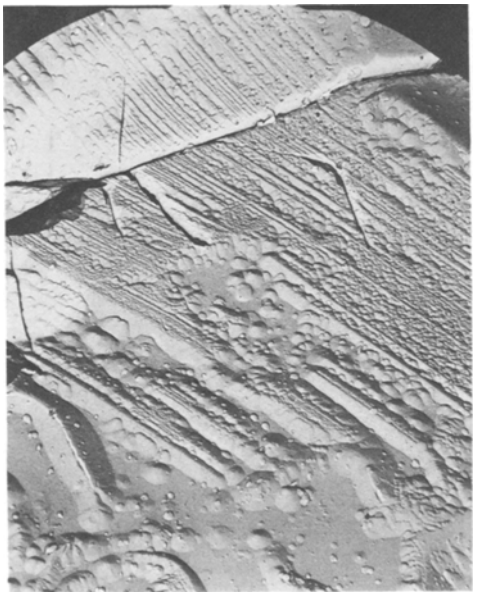

Figure 4 Electron micrograph (replica) of several grains from the hot-pressed BeO deformed at 1.0 GPa (× 5000). Closely spaced pits (lineations) and individual pits indicate high density of dislocations characteristic of intragranular plasticity.

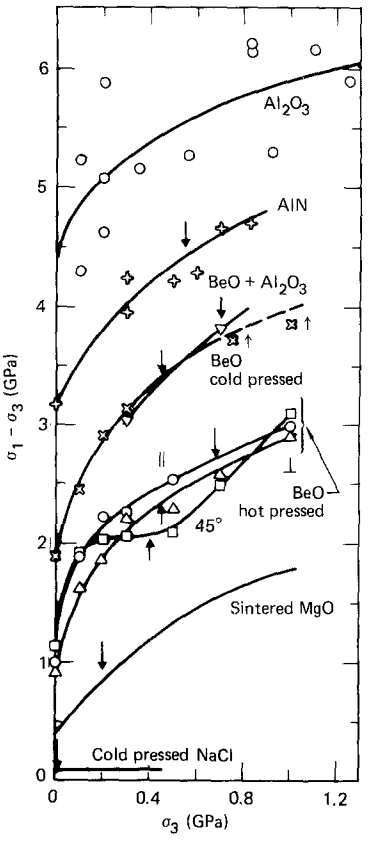

Figure 5 Ultimate strength (maximum $\sigma_1 - \sigma_3$) as a function of σ_3 for several types of BeO, Al_2O_3, AlN, MgO and NaCl. The brittle–ductile (BD) transition pressures are indicated by heavy arrows. Light arrows indicate minimum values of stress difference.

lar to the plane of the initial plate. Thus, in these three cases, compression took place along an axis that was (1) randomly oriented, (2) oriented at 45° to 90°, and (3) oriented at 90° to the *c*-axis maximum, respectively. Note in Figs. 1 to 3, the stress difference $\sigma_1 - \sigma_3$ is plotted against axial strain ϵ_1. Listed by each curve is the value for the confining pressure for that individual test.

In Fig. 1, at the lowest pressure (0.1 MPa), BeO is essentially elastic up to the failure stress of 0.95 GPa. Tensile fracture parallel to σ_1 as well as shear fracture ~30° to σ_1 are dominant under these conditions. As σ_3 increases, this material becomes progressively stronger and more ductile. At the highest pressure, the yield strength has increased by more than a factor of two and the ultimate strength by nearly a factor of three. Work hardening is apparent at $\sigma_3 = 1.0$ GPa. Intracrystalline slip by dislocation motion with consequent pile-up at grain boundaries is the dominant deformation mechanism here, and no fractures are observed (see Fig. 4).

As values of σ_3 are increased from 0.1 to 0.5 GPa, there is a corresponding progressive increase in strain (after the yield point) because of this plastic flow before onset of fracture. At these pressures, limited local fracturing occurs at strains beyond the ultimate strength (maximum ordinate on the stress–strain curve), but as plasticity is enhanced with σ_3, this fracturing decreases. Only when these fractures coalesce does the stress drop catastrophically, as shown in the dashed section of each curve. The brittle–ductile transition pressure, below which brittle fracture dominates and above which ductile flow is controlling, can then be defined on the basis of the observed deformation mechanism as well as on the amount of strain after the yield point and on the overall shape of the stress–strain curve. Results illustrated in Figs. 2 and 3 are quite similar to those shown in Fig. 1. We would then qualitatively place this transition slightly below 0.5 GPa for the BeO tests shown in Figs. 1 and 2 and slightly above 0.6 GPa for those in Fig. 3. For these three orientations, where $\sigma_1 - \sigma_3$ (maximum) is plotted versus σ_3 (see Fig. 5), the approximate brittle–ductile transition pressure is indicated by an arrow.

When the fabrication procedure or the composition used in preparation of the starting material

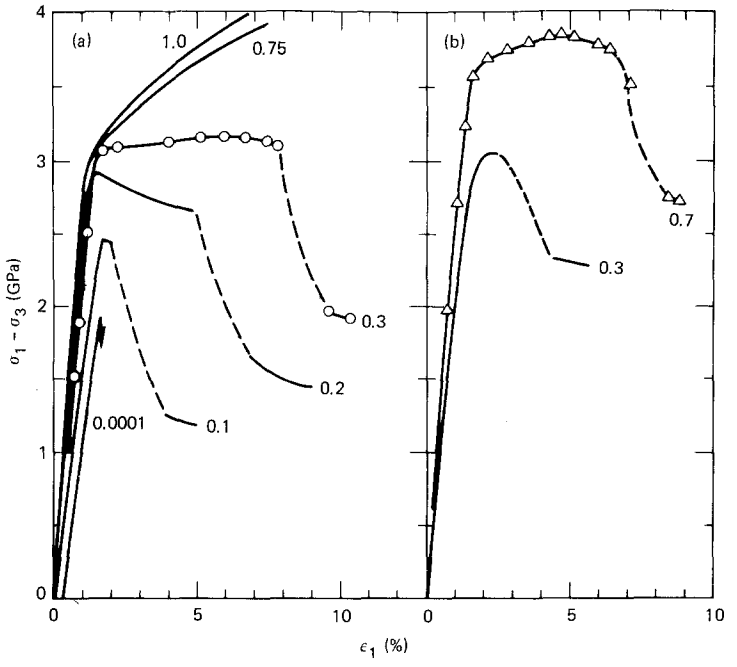

Figure 6 Stress–strain curves for (a) cold-pressed BeO, and (b) cold-pressed BeO + 4 mol % Al_2O_3 with compression normal to parent disc (strain rate from 3 to 7×10^{-5} sec^{-1}). Numbers on curves denote pressure in GPa. Data points seen at 0.3 GPa and 0.7 GPa in (a) and (b) are typical of scatter in stress–strain measurements.

is altered, both strength and ductility are affected. Stress–strain results, similar to those in Figs. 1 to 3, are shown in Fig. 6 for cold-pressed and sintered BeO (30 μm grain size, $< 5\%$ porosity) and for a cold-pressed and sintered BeO containing 4 mol % Al_2O_3 ($\sim 1\%$ porosity). For both of these materials, as was observed for hot-pressed BeO, strength and ductility are enhanced with pressure. However, for cold-pressed and sintered BeO, the initial cold-pressing operation apparently results in a higher strength at any strain and an increased work hardening at the higher pressures. The brittle–ductile transition appears to occur at nearly the same pressure as for the perpendicularly oriented hot-pressed BeO (cf. Figs. 1 and 5). The addition of 4 mol % Al_2O_3 to hot-pressed BeO also increases the strength and work hardening but apparently decreases ductility at any pressure (see Fig. 6), as compared to the hot-pressed material (Fig. 1). Although there are fewer data, the brittle–ductile transition pressure of BeO + Al_2O_3 (Fig. 5) seems slightly higher than observed in the other BeO cases.

The fourth material tested was Al_2O_3 (Table I). Unlike each of the BeO aggregates discussed above, this material remains essentially elastic and brittle at all pressures up to 1.25 GPa. The fracture strength shows considerable scatter but was much higher at all pressures than for any BeO sample. No stress–strain results are shown, but ultimate strengths (at fracture) are included in Fig. 5 for comparison with the BeO materials. The pressure at which this Al_2O_3 becomes ductile is not known, but judging from the results of Bridgman [3], it would probably be in excess of 3 GPa.

The last material investigated was hot-pressed AlN, which has $< 1\%$ porosity. Fig. 7 illustrates

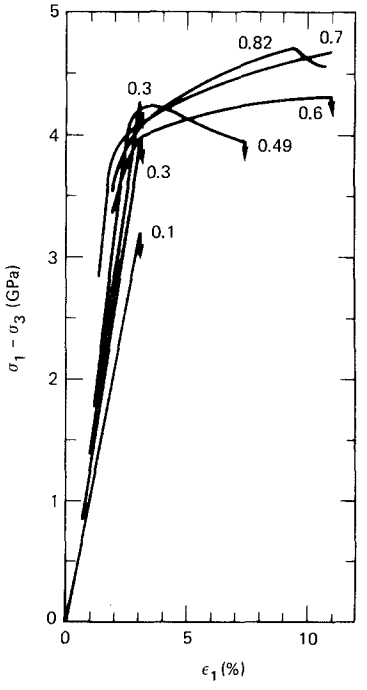

Figure 7 Stress–strain curves for hot-pressed AlN (strain rate from 3 to 7×10^{-5} sec^{-1}). Numbers on curves denote pressure in GPa.

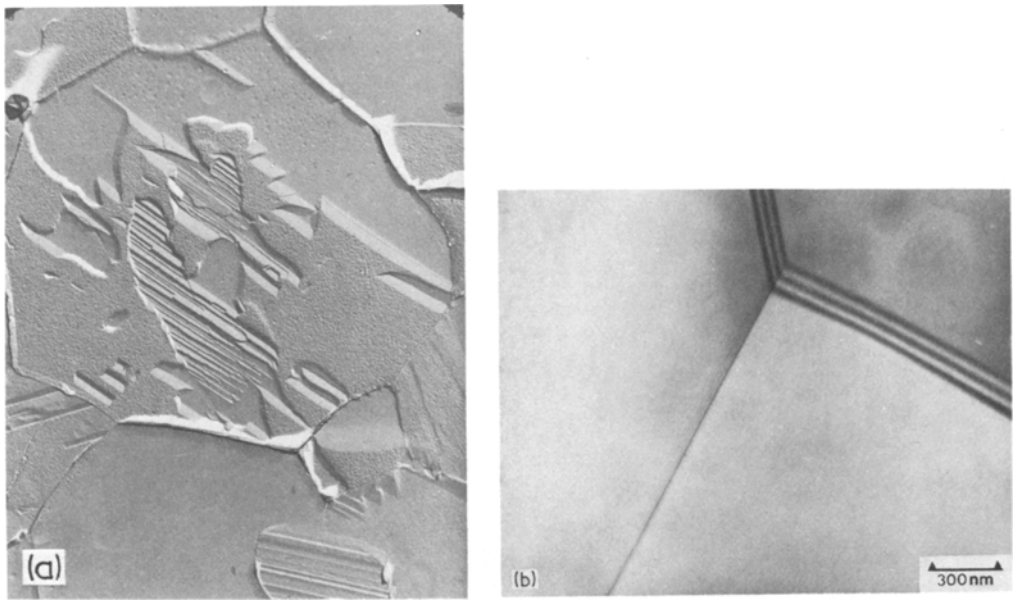

Figure 8 Electron micrographs of grains from AlN material. (a) Grains from initial AlN material (× 5000). Note local twin structures in some grains. (b) Three grains from undeformed AlN (× 60 000). Note absence of any internal structures or pits, suggesting the initial dislocation density is very low. Contrast with Fig. 9. Sample thinned by ion milling.

the stress–strain results at pressures up to 0.82 GPa. Although AlN and BeO show similar changes in work hardening and ductility characteristics with pressure, AlN is considerably stronger. The brittle–ductile transition pressure for AlN is about the same as the average for all BeO samples (Fig. 5). The ultimate strength of AlN lies approximately midway between that of cold-pressed BeO and Al_2O_3 at similar pressures (Fig. 5).

Microscopic evidence supporting the supposition that the change in mechanical response of AlN at high pressure is due to intracrystalline slip by dislocation generation and motion is shown in Figs. 8 and 9. Fig. 8a is an electron micrograph of a replicated surface of a control sample of AlN. The internal regions in many grains show fine twin structures, which do not appear to play any significant role in the high-pressure deformation. This type of twin has been reported previously [12]. Fig. 8b shows a twin-free grain in the AlN and shows the absence of any dislocations before deformation. Fig. 9 is a TEM photograph (0 0 0 1) of a single crystal from the AlN sample that was deformed at 0.7 GPa (see Fig. 7). The strong linear traces (NS, WNW, and ENE) indicate a high concentration of dislocations parallel to the traces of all three *a*-axes. The details of these dislocation structures are still under investigation and will be reported at a later date.

4. Discussion

Figs. 1 to 4 and 6 to 9 demonstrate that the application of moderate to high hydrostatic pressure can play a profound role in the deformation behaviour of BeO and AlN aggregates at room temperature. In such materials, which are

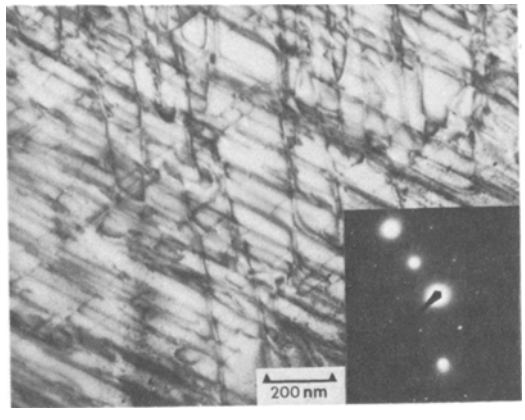

Figure 9 Transmission electron micrograph of AlN grain from aggregate deformed at 0.7 GPa (× 90 000). Plane of photograph is (0 0 0 1), and [1 0 $\bar{1}$ 0] is EW. Note traces of dislocation structures parallel to all three *a*-axes (NS, WNW, and ENE). Sample thinned by ion milling.

ordinarily brittle at ambient pressures, fracture in individual crystals occurs when the critical tensile stress across a potential cleavage plane is exceeded. Thus, the compressive strength of the aggregate is relatively low, and the material is essentially elastic up to the failure stress. The critical resolved shear stresses on potential slip planes are not exceeded under these conditions, because few dislocations are generated or propagated within the crystals. When the fractures from individual crystals grow and coalesce, the deformation is accompanied by a bulk volume increase because of this fracture porosity. However, deformation at high pressure excludes or greatly inhibits any fracture. All changes in shape of the deforming aggregate must then take place through the activation of at least five independent slip systems to preserve volume [13, 14]. In the case of BeO, we are investigating these slip systems at conditions of pressure, temperature, and strain-rate identical to those studied here. As already noted, the operative slip systems for AlN are currently under investigation.

For comparison, we also show ultimate strength data in Fig. 5 for polycrystalline MgO and NaCl, similarly deformed at high pressure [15, 16]. Sodium chloride is extremely weak and completely ductile at pressures in excess of about 5 MPa. Sintered MgO has strength and ductility qualities midway between NaCl and BeO.

The fabrication process to be employed as well as most applications for these polycrystalline materials are dependent on the strength–ductility behaviour under pressure. Some applications also require that either the strength or ductility must remain high at elevated temperatures or at high strain rates. The energy used during fabrication or the ability of the specific material to absorb energy without undergoing catastrophic failure are both directly proportional to these physical properties, that is, to the distortional strain energy and, to a much lesser degree, to the dilatational energy absorbed by the material.

For the uniaxial compressive stress loading used here, distortional strain energy is given by $(1+\nu)/3(\sigma_1-\sigma_3)^2$, where ν is Poisson's ratio [17]. This is equivalent to the product $2/3\ (1+\nu)$ times the area under the stress–strain curve (e.g. Fig. 1), which is $\epsilon_1(\sigma_1-\sigma_3)/2$. Since ν was not determined in our tests under pressure, it is not possible to rigorously determine this initial term. But since ν must range between 0 and 0.5 and more realistically lie between 0.1 and 0.3, this term must range between 0.67 and 1.0 or, as is more likely, between 0.74 and 0.87. In any case the distortional strain energy is approximately equal to $\epsilon_1(\sigma_1-\sigma_3)/2$. Dilatational strain energy is $3/2\ \sigma_1\epsilon_1$ under hydrostatic loading.

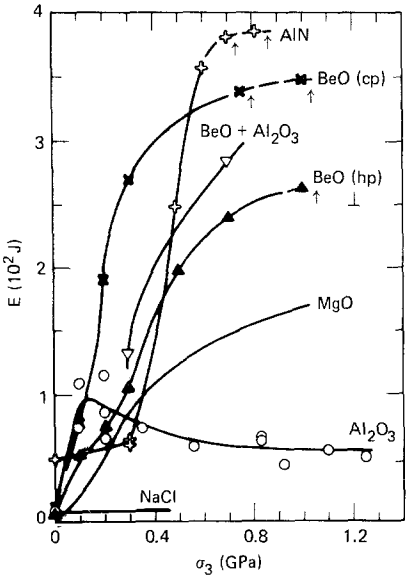

Figure 10 Absorbed energy as a function of σ_3 for various types of BeO, Al_2O_3, AlN, MgO and NaCl (strain rate from 3 to 7×10^{-5} sec^{-1}). Arrows indicate minimum values.

Without considering the absorbed strain energy for the moment, we will suppose each material shown in Fig. 5 is a structural material for use as a coating or a thick facing on a substrate and is designed to resist abrasion or to defeat a punching motion; then, it would at first appear that the material with the least strength (NaCl) would be least desirable while the strongest (Al_2O_3) would be the best. This conclusion would, of course, be tempered somewhat by consideration of the relative strength (hardness) of the indenter and the ceramic facing material as well as by consideration of the pressures and stress differences developed in the vicinity of the punch tip.

However, from the standpoint of distortional strain energy expended by the punch in penetrating the ceramic, the ordering suggested by Fig. 5 no longer holds. This can be inferred from the area under the stress–strain curves shown in Figs. 1 to 3, 6, and 7 but is perhaps best illustrated in Fig. 10 where this area is plotted versus pressure. Except for a somewhat confused region at pressures less than about 0.3 GPa, the ordering is similar

to that of Fig. 5: NaCl seems the least desirable and AlN the most desirable. The outstanding exception (see Figs. 5 and 10) is Al_2O_3 – the *only* material that does not undergo a brittle-to-ductile transition within the pressure range investigated. From the standpoint of this energy argument, Al_2O_3 does not appear to be as good as MgO but, at moderate to high pressures, is still much better than NaCl.

The peculiar shape of the Al_2O_3 curve in Fig. 10 is directly related to the increase in Young's modulus with pressure. Thus, even though the stress increases with pressure, the resulting area is lowered by the dominating modulus increase. Strength, as well as modulus, also increases for all other materials shown in Figs. 5 and 10, but the onset of ductility at low to intermediate pressures more than offsets the modulus effect when the approximate distortional strain energy is computed. If we were to include the effect of absorbed dilatational strain energy in Fig. 10, the relative position of each material would not change. The calculated increase for NaCl at 0.4 GPa would be about 0.15×10^2 J, an increment of about a factor of 2. The increase in Al_2O_3, MgO, and BeO would be insignificant, less than 0.05×10^2 J as calculated from published compressibility data [18]. No data are available for AlN, but we would expect this volumetric strain correction to be similar to that of the above oxides. In Fig. 10, the arrows at the highest pressure on the curves for AlN, cold-pressed BeO, and hot-pressed BeO indicate only *minimum* values; the deformation test was terminated before fracture (see Figs. 1, 6 and 7).

A comparison of the ceramics shown in Fig. 10 suggests that for high indentation stresses, AlN and perhaps cold-pressed BeO would be two prime materials for certain structural applications. Further, hot-pressed BeO and perhaps MgO would be intermediate materials, while Al_2O_3 and NaCl would be least desirable. However, considerations of other physical–chemical properties are sometimes important or overriding. These might include density, elastic moduli, toxicity, and mechanical properties of the indenter. Cost, general availability or strategic considerations are also sometimes important. Aluminium nitride then would seem a most attractive new material.

All data and discussion presented thus far have been on the mechanical behaviour of materials at strain rates of 10^{-4} sec^{-1} and at high pressures. However, in certain applications (i.e. high-velocity projectile impact), loading rates may be higher by 10^6 to 10^8, and stresses under the projectile may exceed 15 GPa. Laboratory testing of many silicate and carbonate rock materials at high pressures and strain rates demonstrates that ductility is decreased with strain rate while compressive strength is increased [6, 7, 19–21]. Qualitatively, these as well as other studies show that strength is increased by ~ 10% per 10-fold increase in rate and that ductility is lowered on the order of 1% (in strain) per 10-fold increase in rate.

The few tests we have made on cold-pressed BeO at a strain rate of approximately 10 sec^{-1} and at moderate pressures confirm these results reported for rock materials. We are not aware of similar data for the remaining materials discussed here. However, we would expect that at much higher loading rates (impact), an absorbed energy–pressure diagram similar to Fig. 10 would indicate improved energy absorption at low pressure for each material. At moderate pressures, we would expect each material except NaCl and Al_2O_3 to show a degraded absorption. The absorption for these last two materials would be increased considerably. At high pressures, AlN, BeO, and MgO should show increased absorption consistent with that for NaCl and Al_2O_3.

Considerable caution should be exercised when inferring ballistic performance from curves such as those shown in Fig. 10, because other factors can be important (e.g. physical properties of the projectile and tensile strength of the armour).

5. Conclusions

(1) The high-pressure mechanical properties of BeO, AlN, and Al_2O_3 aggregates were evaluated at strain rates of 10^{-4} sec^{-1} and at room temperature.

(2) All materials except Al_2O_3 exhibit an increase both in compressive strength and ductility with pressure. Several types of BeO undergo a brittle–ductile transition by suppression of fracture with increasing dislocation-generation migration at pressures of 0.4 to 0.7 GPa. At about 0.55 GPa, AlN exhibits an identical behaviour.

(3) Brittle fracture dominates in Al_2O_3 up to the highest pressure investigated (1.25 GPa).

(4) For applications requiring compressive strength at high pressures, Al_2O_3 is superior and is followed closely by AlN and BeO.

(5) Use of these materials in applications where energy absorption at moderate strain rates is of

overriding importance, AlN is superior and is closely followed by BeO, with Al_2O_3 being last.

Acknowledgements

We gratefully acknowledge the efforts of J. Mitchell, C. Echer, and S. Digiallonardo in obtaining the excellent electron micrographs shown in Figs. 8 and 9. This work was performed under the auspices of the US Department of Energy at Lawrence Livermore Laboratory under contract No. W-7405-Eng-48.

References

1. M. L. WILKINS, C. F. CLINE and C. A. HONODEL, Fourth Progress Report of Light Armor Program, Lawrence Livermore Laboratory, Rept. UCRL-50694 (1969).
2. T. VON KARMAN, *Z. Ver. Deutsch. Ingenieure* **55** (1911) 1749.
3. P. W. BRIDGMAN, "Studies in Large Plastic Flow and Fracture" (McGraw-Hill, New York, 1952).
4. D. T. GRIGGS, *J. Geol.* **44** (1936) 541.
5. H. C. HEARD and C. B. RALEIGH, *Geol. Soc. Am. Bull.* **83** (1972) 935.
6. H. C. HEARD and N. L. CARTER, *Amer. J. Sci.* **266** (1968) 1.
7. J. HANDIN, H. C. HEARD and J. M. MAGOUIRK, *J. Geophys. Res.* **72** (1968) 611.
8. G. A. JEFFREY, G. S. PARRY and R. L. MOZZI, *J. Chem. Phys.* **25** (1956) 1024.
9. D. K. SMITH, H. W. NEWKIRK and J. S. KAHN, *J. Electrochem. Soc.* **111** (1964) 78.
10. C. F. CLINE and J. S. KAHN, *ibid.* **110** (1963) 773.
11. R. N. SCHOCK, H. C. HEARD and D. R. STEPHENS, *J. Geophys. Res.* **78** (1973) 5922.
12. S. HORIUCHI and T. ISHII, *J. Crystal Growth* **21** (1974) 17.
13. R. VON MISES, *Z. Angew. Math. Mech.* **8** (1928) 161.
14. G. I. TAYLOR, *J. Inst. Metals* **62** (1938) 307.
15. H. C. HEARD, A. E. ABEY, B. P. BONNER and A. DUBA, "Stress–Strain Behaviour of Polycrystalline NaCl to 3.2 GPa", Lawrence Livermore Laboratory, Rept. UCRL-51743 (1975).
16. M. S. PATERSON and C. W. WEAVER, *J. Amer. Ceram. Soc.* **53** (1970) 463.
17. S. TIMOSHENKO, "Strength of Materials II" (Van Nostrand, Princeton, New Jersey, 1956).
18. F. BIRCH, "Handbook of Physical Constants" (Memoir 97), edited by S. P. Clark (Geological Society of America, New York, 1966) pp. 97–173.
19. S. SERDENGECTI and G. D. BOOZER, "Proceedings of the Fourth Symposium on Rock Mechanics" (Intersociety Committee for Rock Mechanics and Pennsylvania State University, 1961) p. 83.
20. U. S. LINDHOLM, L. M. YEAKLEY and A. NAGY, *Int. J. Rock Mech. Min. Sci.* **11** (1974) 181.
21. J. M. LOGAN and J. HANDIN, "Proceedings of the Twelfth Symposium on Rock Mechanics" (US National Committee for Rock Mechanics and the University of Missouri, 1970) p. 167.

Received 26 April and accepted 13 September 1979